J. Phys. B: At. Mol. Opt. Phys. **42** (2009) 215204 (5pp) doi:10.1088/0953-4075/42/21/215204

Electron-impact double ionization of magnesium

M S Pindzola[1], J A Ludlow[1], F Robicheaux[1], J Colgan[2] and D C Griffin[3]

[1] Department of Physics, Auburn University, Auburn, AL, USA
[2] Theoretical Division, Los Alamos National Laboratory, Los Alamos, NM, USA
[3] Department of Physics, Rollins College, Winter Park, FL, USA

Received 24 July 2009, in final form 9 September 2009
Published 27 October 2009
Online at stacks.iop.org/JPhysB/42/215204

Abstract
Theory and experiment are compared for the electron-impact double ionization of Mg. Direct ionization cross sections, involving the simultaneous ionization of both 3s electrons, are calculated using a non-perturbative time-dependent close-coupling method. Indirect ionization cross sections, involving the ionization of either a 2p or 2s electron followed by autoionization, are calculated using a perturbative time-independent distorted-wave method. At low energies the direct ionization cross sections are found to be in good agreement with experiments, while at the higher energies the indirect ionization cross sections are also found to be in good agreement with experiments.

(Some figures in this article are in colour only in the electronic version)

1. Introduction

Electron-impact double ionization of atoms remains a challenging computational task for *ab initio* theory. Cross sections for light atoms are dominated by a direct process in which the incident electron stimulates the simultaneous emission of two electrons, resulting in a four-body Coulomb breakup problem. Work on the electron-impact double ionization of helium has found good agreement between non-perturbative time-dependent close-coupling calculations [1, 2] and absolute experimental measurements [3] for total cross sections. Recent reaction microscope experiments have provided energy and angle differential cross sections for the electron-impact double ionization of helium at incident energies just above threshold [4, 5]. Theoretical calculations based on a six interacting Coulomb waves method [4], a first Born implementation of the converged close-coupling method [4] and a time-dependent close-coupling method [6], have found good agreement between theory and experiment for pentuple differential cross section shapes, but not absolute magnitudes.

On the other hand, electron-impact double-ionization cross sections for medium to heavy atoms are generally found to be dominated by an indirect process in which the incident electron ionizes an inner-shell electron, followed by autoionization of the excited atomic ion. Early theoretical and experimental studies of the electron-impact double ionization of inert gas atomic ions found that the indirect ionization–autoionization mechanism dominates total double-ionization cross sections [7]. Non-perturbative calculations for the electron-impact single ionization of loosely bound excited states of hydrogen [8, 9] and helium [10, 11] have shown that perturbative distorted-wave calculations are quite inaccurate. However, for the ionization of the tightly bound inner shell states in moderate to heavy atoms, the perturbative distorted-wave method should be reasonably accurate [12].

In this paper, we extend our recent non-perturbative calculations for the electron-impact single ionization of Mg [13] to examine the electron-impact double ionization of Mg. Although early experimental measurements [14, 15] of the double ionization cross section for Mg differed by a factor of 3, later experiments [16, 17] are in reasonable agreement with each other from threshold to 700 eV. From the double-ionization threshold of 22.7 eV to the 2p inner shell single-ionization threshold of 57 eV, we carried out calculations for the double ionization of both 3s electrons using the non-perturbative time-dependent close-coupling method. Above the 2p inner shell single-ionization threshold of 57 eV, we carried out calculations for the single ionization of the 2p and 2s electrons using the perturbative time-independent distorted-wave method. Comparisons are made with experiments [16, 17] from threshold to 500 eV.

The remainder of the paper is organized as follows. In section 2, we review the time-independent distorted-wave

and time-dependent close-coupling methods. In section 3, we apply the distorted-wave and close-coupling methods to the calculation of the electron-impact double ionization cross section of Mg. In section 4, we conclude with a summary and an outlook for future work. Unless otherwise stated, all quantities are given in atomic units.

2. Theory

2.1. Time-independent distorted-wave method

The configuration-average distorted-wave expression for the electron-impact single ionization cross section of the $(n_t l_t)^{w_t}$ subshell of any atom is given by [18]

$$\sigma = \frac{16 w_t}{k_i^3} \int_0^E \frac{\mathrm{d}\epsilon_e}{k_e k_f} \sum_{l_i, l_e, l_f} (2l_i + 1)(2l_e + 1)(2l_f + 1) \times \mathcal{P}(n_t l_t, k_i l_i, k_e l_e, k_f l_f), \tag{1}$$

where the linear momentum (k_i, k_e, k_f) and the angular momentum (l_i, l_e, l_f) quantum numbers correspond to the incoming, ejected and outgoing electrons, respectively. The total energy $E = \epsilon_i - I = \epsilon_e + \epsilon_f$, where I is the subshell ionization energy and $\epsilon = \frac{k^2}{2}$. The first-order perturbation theory expression for the scattering probability $\mathcal{P}(n_t l_t, k_i l_i, k_e l_e, k_f l_f)$ is given in terms of standard $3j$ and $6j$ symbols and radial Slater integrals [18].

The radial distorted-waves, $P_{kl}(r)$, needed to evaluate the Slater integrals are solutions to the time-independent non-relativistic radial Schrödinger equation given by

$$\left(-\frac{1}{2}\frac{\mathrm{d}^2}{\mathrm{d}r^2} + \frac{l(l+1)}{2r^2} + V(r) - \frac{k^2}{2} \right) P_{kl}(r) = 0. \tag{2}$$

The atomic potential is given by

$$V(r) = -\frac{Z}{r} + \sum_{nl} \left(\int_0^\infty \frac{P_{nl}^2(r')}{r_>} \mathrm{d}r' - \alpha \left[\frac{24 \rho_{nl}(r)}{\pi} \right]^{\frac{1}{3}} \right), \tag{3}$$

where Z is the atomic number, $r_> = \max(r, r')$, and α is a parameter determined by removal energies. The bound radial orbitals, $P_{nl}(r)$, and radial probability densities, $\rho_{nl}(r) = \frac{P_{nl}^2(r)}{4\pi r^2}$, are calculated using a Hartree–Fock atomic structure code [19]. The incident and scattered electron continuum orbitals are calculated in a V^N potential, while the ejected electron continuum orbitals are calculated in a V^{N-1} potential, where N is the number of target electrons. The continuum normalization for all distorted waves is 1 times a sine function.

2.2. Time-dependent close-coupling method

For electron-impact single and double ionization of an atom with two active electrons, the time-dependent non-relativistic Schrödinger equation is given by

$$\mathrm{i}\frac{\partial \Psi(\vec{r}_1, \vec{r}_2, \vec{r}_3, t)}{\partial t} = H(\vec{r}_1, \vec{r}_2, \vec{r}_3)\Psi(\vec{r}_1, \vec{r}_2, \vec{r}_3, t), \tag{4}$$

where

$$H(\vec{r}_1, \vec{r}_2, \vec{r}_3) = \sum_i^3 \left(-\frac{1}{2}\nabla_i^2 + V(r_i) \right) + \sum_{i<j}^3 \frac{1}{|\vec{r}_i - \vec{r}_j|}. \tag{5}$$

The atomic potential is given by

$$V(r) = -\frac{Z}{r} + U_{\mathrm{core}}(r), \tag{6}$$

where $U_{\mathrm{core}}(r)$ is a core pseudo-potential [20].

Expanding the wavefunction in coupled spherical harmonics:

$$\Psi(\vec{r}_1, \vec{r}_2, \vec{r}_3, t) = \sum_{l_1, l_2, L, l_3} \frac{P^{\mathcal{LS}}_{l_1 l_2 L l_3}(r_1, r_2, r_3, t)}{r_1 r_2 r_3} \times Y_{((l_1, l_2)L, l_3)\mathcal{L}}(\hat{r}_1, \hat{r}_2, \hat{r}_3), \tag{7}$$

and substitution into equation (4) yields the time-dependent close-coupled equations [1]:

$$\mathrm{i}\frac{\partial P^{\mathcal{LS}}_{l_1 l_2 L l_3}(r_1, r_2, r_3, t)}{\partial t} = T_{l_1 l_2 l_3}(r_1, r_2, r_3) P^{\mathcal{LS}}_{l_1 l_2 L l_3}(r_1, r_2, r_3, t) + \sum_{l_1', l_2', L', l_3'} \sum_{i<j}^3 W^{\mathcal{L}}_{l_1 l_2 L l_3, l_1' l_2' L' l_3'}(r_i, r_j) P^{\mathcal{LS}}_{l_1' l_2' L' l_3'}(r_1, r_2, r_3, t), \tag{8}$$

where

$$T_{l_1 l_2 l_3}(r_1, r_2, r_3) = \sum_i^3 \left(-\frac{1}{2}\frac{\partial^2}{\partial r_i^2} + \frac{l_i(l_i+1)}{2r_i^2} + V(r_i) \right) \tag{9}$$

and $W^{\mathcal{L}}_{l_1 l_2 L l_3, l_1' l_2' L' l_3'}(r_i, r_j)$ are two-body coupling operators.

The correlated wavefunction for the ground state of an atom with two active electrons is obtained by relaxation of the time-dependent non-relativistic Schrödinger equation in imaginary time ($\tau = \mathrm{i}t$). The time-dependent close-coupled equations for the radial wavefunctions are given by

$$-\frac{\partial \bar{P}^{LS}_{l_1 l_2}(r_1, r_2, \tau)}{\partial \tau} = T_{l_1 l_2}(r_1, r_2) \bar{P}^{LS}_{l_1 l_2}(r_1, r_2, \tau) + \sum_{l_1', l_2'} W^{L}_{l_1 l_2, l_1' l_2'}(r_1, r_2) \bar{P}^{LS}_{l_1' l_2'}(r_1, r_2, \tau). \tag{10}$$

The initial condition for electron scattering from an atom with a closed $(ns)^2\ {}^1\mathrm{S}$ outer subshell is given by [1]

$$P^{\mathcal{LS}}_{l_1 l_2 L l_3}(r_1, r_2, t = 0) = \sum_l \bar{P}^{00}_{ll}(r_1, r_2, \tau \to \infty) \times F_{k_0 \mathcal{L}}(r_3) \delta_{l_1, l} \delta_{l_2, l} \delta_{L, 0} \delta_{l_3, \mathcal{L}}, \tag{11}$$

where the Gaussian radial wavepacket, $F_{k_0 \mathcal{L}}(r)$, has a propagation energy of $\frac{k_0^2}{2}$.

Following propagation of the time-dependent close-coupled equations of equation (8), the coupled radial wavefunctions are projected onto fully antisymmetric products of one-electron spin orbitals with $\left(s_1 = s_2 = s_3 = \frac{1}{2}\right)$ to yield various scattering probability amplitudes. The single-ionization probability amplitudes:

$$\mathcal{A}_{0 s_1 l_2 s_2 L S l_3 s_3 \mathcal{L} \mathcal{S}}(ns, k_2 l_2, k_3 l_3) \tag{12}$$

are found by weighted sums over permutations of

$$\int_0^\infty \mathrm{d}r_1 \int_0^\infty \mathrm{d}r_2 \int_0^\infty \mathrm{d}r_3 P_{ns}(r_1) P_{k_2 l_2}(r_2) P_{k_3 l_3}(r_3) \times P^{\mathcal{LS}}_{s l_2 L l_3}(r_1, r_2, r_3, t \to \infty), \tag{13}$$

where the box normalized continuum orbitals are calculated in a V^{N-1} potential. The double-ionization probability amplitudes:

$$\mathcal{A}_{l_1 s_1 l_2 s_2 L S l_3 s_3 \mathcal{L}\mathcal{S}}(k_1 l_1, k_2 l_2, k_3 l_3) \tag{14}$$

are found by weighted sums over permutations of

$$\int_0^\infty \mathrm{d}r_1 \int_0^\infty \mathrm{d}r_2 \int_0^\infty \mathrm{d}r_3 P_{k_1 l_1}(r_1) P_{k_2 l_2}(r_2) P_{k_3 l_3}(r_3) \times P^{\mathcal{L}\mathcal{S}}_{l_1 l_2 L l_3}(r_1, r_2, r_3, t \to \infty), \tag{15}$$

where the box normalized continuum orbitals are calculated in a V^{N-2} potential. We found that a simple restriction of the radial integrals found in expressions (13) and (15) over a range from $r_i = 5.0$ to $r_i = \infty$ greatly reduced contamination from the continuum piece of the two-electron target wavefunction.

Finally, the single-ionization cross section is given by

$$\sigma_{\mathrm{ion}} = \frac{\pi}{2k_0^2} \int_0^\infty \mathrm{d}k_2 \int_0^\infty \mathrm{d}k_3 \sum_{\mathcal{L},\mathcal{S}} (2\mathcal{L}+1)(2\mathcal{S}+1) \times \sum_{L,S} \sum_{l_2,l_3} \left| \mathcal{A}_{0 s_1 l_2 s_2 L S l_3 s_3 \mathcal{L}\mathcal{S}}(n s, k_2 l_2, k_3 l_3) \right|^2, \tag{16}$$

while the double-ionization cross section is given by

$$\sigma_{\mathrm{dion}} = \frac{\pi}{2k_0^2} \int_0^\infty \mathrm{d}k_1 \int_0^\infty \mathrm{d}k_2 \int_0^\infty \mathrm{d}k_3 \sum_{\mathcal{L},\mathcal{S}} (2\mathcal{L}+1)(2\mathcal{S}+1) \times \sum_{L,S} \sum_{l_1,l_2,l_3} \left| \mathcal{A}_{l_1 s_1 l_2 s_2 L S l_3 s_3 \mathcal{L}\mathcal{S}}(k_1 l_1, k_2 l_2, k_3 l_3) \right|^2. \tag{17}$$

3. Results

Electron-impact single-ionization cross sections for the $1s^2 2s^2 2p^6 3s^2$ ground configuration of Mg were carried out for the 3s, 2p and 2s subshells using the perturbative time-independent distorted-wave (DW) method described in section 2.1. The Hartree–Fock ionization potentials are found to be $I_{3s} = 7.3$ eV, $I_{2p} = 57$ eV and $I_{2s} = 99$ eV, while the peak cross sections are found to be $\sigma_{3s} = 600$ Mb, $\sigma_{2p} = 22$ Mb and $\sigma_{2s} = 2.0$ Mb, where 1.0 Mb = 1.0×10^{-18} cm^2. The 3s subshell cross section contributes to the single ionization of Mg, while the 2p and 2s subshell cross sections, through the indirect process of ionization–autoionization, contribute to the double ionization of Mg. We note that the branching ratio for autoionization in the neutral Mg atom is assumed to be 1. In figure 1 of our previous work [13], the perturbative distorted-wave results for the single ionization of Mg were found to be 50% above the non-perturbative R-matrix and close-coupling results at the peak of the cross section. In figure 1 of this work, the perturbative distorted-wave results for the double ionization of Mg are found to be in good agreement with experimental measurements [16, 17] at the peak of the cross section.

Electron-impact single- and double-ionization cross sections for the $3s^2$ outer subshell of ground-state Mg were carried out using the non-perturbative time-dependent close-coupling (TDCC) method described in section 2.2. Using a 192 × 192 point numerical lattice with a uniform mesh spacing of $\Delta r = 0.20$ and a core pseudo-potential for the $1s^2 2s^2 2p^6$ ground configuration of Mg^{2+} [20], relaxation of the TDCC equations of equation (10) in imaginary time yielded a correlated $3s^2$ radial wavefunction with an ionization potential of $I_d = 22.3$ eV, compared to the experimental value of $I_d = 22.7$ eV [21]. The initial condition of equation (11) uses the correlated $3s^2$ radial wavefunctions for $l = 0$–3 and radial wavepackets with initial energies $\epsilon_0 = 35$ eV, 45 eV and 55 eV.

Using a 192 × 192 × 192 point numerical lattice with a uniform mesh spacing of $\Delta r = 0.20$, the TDCC equations of equation (8) were propagated in real time for $\mathcal{L} = 0$–5 and $\mathcal{S} = \frac{1}{2}$ total symmetries. Electron-impact single-ionization partial wave cross sections for Mg at an incident energy of 35 eV are given in column 2 of table 1. The third column of table 1 is the number of $l_1 l_2 L l_3$ coupled channels, while the fourth column is the number of $0 s_1 l_2 s_2 L S l_3 s_3$ projection states needed to calculate the single-ionization probability amplitudes found in the cross section expression of equation (16). For comparison, we also present in table 1 the 3s subshell distorted-wave partial wave cross sections, the TDCC-2D partial wave cross sections and the number of $l_1 l_2$ coupled channels used in previous work [13] for the electron-impact single ionization of Mg in columns 5–7. The TDCC-3D and TDCC-2D partial cross sections are found to be in

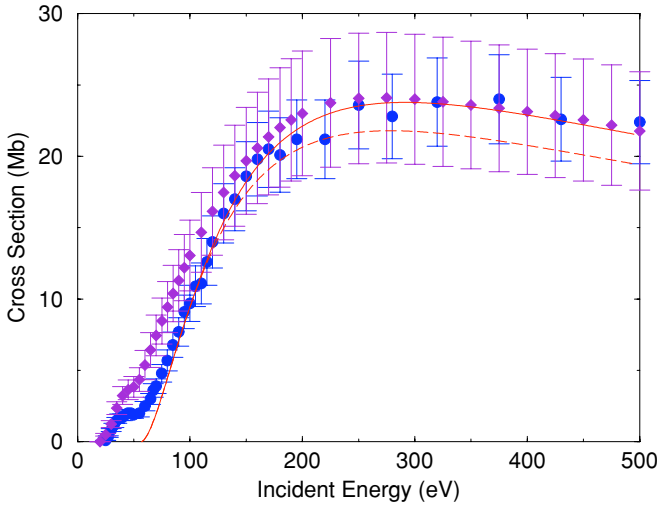

Figure 1. Electron-impact double ionization of Mg. Solid line: perturbative DW calculations for indirect 2s and 2p ionization–autoionization, dashed line: perturbative DW calculations for indirect 2p ionization–autoionization, solid circles: experiment [16], solid diamonds: experiment [17] (1.0 Mb = 1.0×10^{-18} cm^2).

Table 1. Electron-impact single-ionization partial wave cross sections (in Mb) for Mg at an incident energy of 35 eV. TDCC-3D: present calculations, DW: past calculations [13], TDCC-2D: past calculations [13] (1 Mb = 1.0×10^{-18} cm^2).

$\mathcal{L}$	TDCC-3D	Channels	Projections	DW	TDCC-2D	Channels
0	3.9	11	6	6.1	3.0	9
1	14.2	21	4	31.7	13.3	16
2	30.0	23	6	65.2	37.3	22
3	42.3	49	6	64.9	48.9	26
4	43.5	60	8	52.1	43.7	29
5	43.6	81	8	50.4	42.7	30

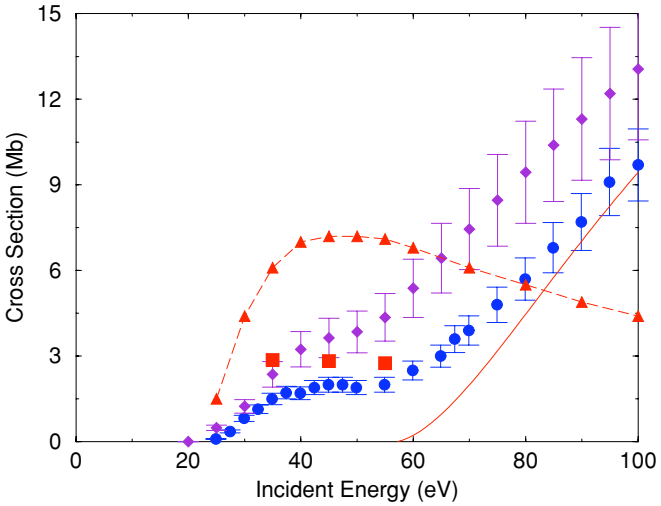

Figure 2. Electron-impact double ionization of Mg near threshold. Solid squares: non-perturbative TDCC calculations for direct double ionization, solid line: perturbative DW calculations for indirect 2s and 2p ionization–autoionization, solid triangles connected by dashed line: binary encounter calculations for direct double ionization [22], solid circles: experiment [16], solid diamonds: experiment [17] (1.0 Mb = 1.0×10^{-18} cm^2).

reasonable agreement, while the TDCC and DW cross sections begin to achieve agreement for the higher partial waves.

The same $192 \times 192 \times 192$ point numerical lattice propagated TDCC equations of equation (8), with projection states $l_1 s_1 l_2 s_2 L S l_3 s_3$ ranging from 10 for $\mathcal{L} = 0$ to 46 for $\mathcal{L} = 5$, were used to calculate the double-ionization probability amplitudes found in the cross section expression of equation (17). The total $\mathcal{L} = 0$–5 electron-impact double-ionization cross sections were found to be 2.2 Mb at an incident energy of 35 eV, 2.1 Mb at an incident energy of 45 eV and 2.0 Mb at an incident energy of 55 eV. The cross sections were extrapolated to higher $\mathcal{L}$ using a nonlinear angular momentum fitting expression given by

$$\sigma(\mathcal{L}) = c_1 \mathcal{L}^{c_2} \, \mathrm{e}^{-\frac{2I_\mathrm{d}}{E}\mathcal{L}}, \tag{18}$$

where I_d is the double ionization potential, E is the incident energy and c_1, c_2 are fitting coefficients. The fitting expression was tested using DW partial cross sections, known from $l_i = 0$ to 50. The total double-ionization cross sections are found to be 2.9 Mb at an incident energy of 35 eV, 2.8 Mb at an incident energy of 45 eV and 2.7 Mb at an incident energy of 55 eV. In figure 2, the non-perturbative time-dependent close-coupling results for the double ionization of Mg are found to be in good agreement with experimental measurements [16, 17] between the double-ionization threshold at $I_\mathrm{d} = 22.7$ eV and the onset of indirect ionization–autoionization contributions at $I_{2\mathrm{p}} = 57$ eV.

Semi-empirical binary encounter (BE) calculations [22] for direct double ionization of the $3s^2$ subshell, also shown in figure 2, are found to be a factor of 2.5 times higher at the peak of the cross section than the TDCC results. Additional BE calculations [22] for direct simultaneous ionization of 3s and 2p electrons, starting at 80 eV, report a peak cross section of 9.1 Mb at an incident energy of 140 eV. The BE cross sections for the direct double ionization of Mg, when added to our DW cross sections for indirect ionization–autoionization, would produce a total cross section well above the more recent experimental measurements [16, 17].

4. Summary

In conclusion, we have carried out non-perturbative TDCC and perturbative DW calculations for the electron-impact double ionization of the magnesium atom. The perturbative DW calculations for indirect ionization–autoionization contributions, coming from single ionization of the 2p and 2s inner subshells, are found to be in good agreement with experimental measurements [16, 17] near the peak of the cross section at 300 eV incident energy. The non-perturbative TDCC calculations for direct contributions, coming from simultaneous ionization of the $3s^2$ subshell, are also found to be in good agreement with experimental measurements [16, 17] at low incident energies. In the future, we plan to apply the TDCC method to investigate the strength of the direct double-ionization mechanism for other atoms, like Be and Ca. We also plan to continue our work [6] on the TDCC calculation of pentuple energy and angle differential cross sections for the electron-impact double ionization of helium and the alkaline earth atoms.

Acknowledgments

This work was supported in part by grants from the US Department of Energy and the US National Science Foundation. Computational work was carried out at the National Energy Research Scientific Computing Center in Oakland, California and at the National Center for Computational Sciences in Oak Ridge, Tennessee.

References

[1] Pindzola M S, Robicheaux F, Colgan J, Witthoeft M C and Ludlow J A 2004 *Phys. Rev.* A **70** 032705
[2] Pindzola M S, Robicheaux F and Colgan J 2007 *Phys. Rev.* A **76** 024704
[3] Shah M B, Elliott D S, McCallione P and Gilbody H B 1988 *J. Phys. B: At. Mol. Opt. Phys.* **21** 2751
[4] Durr M, Dorn A, Ullrich J, Cao S P, Czasch A, Kheifets A S, Gotz J R and Briggs J S 2007 *Phys. Rev. Lett.* **98** 193201
[5] Ren X, Dorn A and Ullrich J 2008 *Phys. Rev. Lett.* **101** 093201
[6] Pindzola M S, Robicheaux F and Colgan J 2008 *J. Phys. B: At. Mol. Opt. Phys.* **41** 235202
[7] Pindzola M S, Griffin D C, Bottcher C, Crandall D H, Phaneuf R A and Gregory D C 1984 *Phys. Rev.* A **29** 1749
[8] Bartschat K and Bray I 1996 *J. Phys. B: At. Mol. Opt. Phys.* **29** L577
[9] Griffin D C, Ballance C P, Pindzola M S, Robicheaux F, Loch S D, Ludlow J A, Witthoeft M C, Colgan J, Fontes C J and Schultz D R 2005 *J. Phys. B: At. Mol. Opt. Phys.* **38** L199
[10] Bray I and Fursa D V 1995 *J. Phys. B: At. Mol. Opt. Phys.* **28** L197
[11] Colgan J and Pindzola M S 2002 *Phys. Rev.* A **66** 062707
[12] Colgan J, Fontes C J and Zhang H L 2006 *Phys. Rev.* A **73** 062711
[13] Ludlow J A, Ballance C P, Loch S D, Pindzola M S and Griffin D C 2009 *Phys. Rev.* A **79** 032715

[14] Okudaira S, Kaneko Y and Kanomata I 1970 *J. Phys. Soc. Japan* **28** 1536
[15] Karstensen F and Schneider M 1978 *J. Phys. B: At. Mol. Phys.* **11** 167
[16] McCallion P, Shah M B and Gilbody H B 1992 *J. Phys. B: At. Mol. Phys.* **25** 1051
[17] Boivin R F and Srivastava S K 1998 *J. Phys. B: At. Mol. Opt. Phys.* **31** 2381
[18] Pindzola M S, Griffin D C and Bottcher C 1986 *Atomic Processes in Electron–Ion and Ion–Ion Collisions (NATO ASI B* vol 145) (New York: Plenum) p 75
[19] Cowan R D 1981 *The Theory of Atomic Structure and Spectra* (Berkeley, CA: University of California Press)
[20] Wadt W R and Hay P J 1985 *J. Chem. Phys.* **82** 284
[21] See http://physics.nist.gov/PhysRefData
[22] Jha L K and Roy B N 2002 *Eur. Phys. J.* D **20** 5